

Determination of the p-spray profile for n⁺p silicon sensors using a MOSFET

E. Fretwurst, E. Garutti, R. Klanner*, I. Kopsalis, J. Schwandt, M. Weberpals

*Institute for Experimental Physics, University of Hamburg,
Luruper Chaussee 147, D 22761, Hamburg, Germany.*

Abstract

The standard technique to electrically isolate the n⁺ implants of segmented silicon sensors fabricated on high-ohmic p-type silicon are p⁺-implants. Although the knowledge of the p⁺-implant dose and of the doping profile is highly relevant for the understanding and optimisation of sensors, this information is usually not available from the vendors, and methods to obtain it are highly welcome. The paper presents methods to obtain this information from circular MOSFETs fabricated as test structures on the same wafer as the sensors. Two circular MOSFETs, one with and one without a p⁺-implant under the gate, are used for this study. They were produced on Magnetic Czochralski silicon doped with $\approx 3.5 \cdot 10^{12} \text{ cm}^{-2}$ of boron and $\langle 100 \rangle$ crystal orientation. The drain-source current as function of gate voltage for different back-side voltages is measured at a drain-source voltage of 50 mV in the linear MOSFET region, and the values of threshold voltage and mobility extracted using the standard MOSFET formulae. To determine the bulk doping, the implantation dose and profile from the data, two methods are used, which give compatible results. The doping profile, which varies between $3.5 \cdot 10^{12} \text{ cm}^{-3}$ and $2 \cdot 10^{15} \text{ cm}^{-3}$ for the MOSFET with p⁺-implant, is determined down to a distance of a fraction of a μm from the Si-SiO₂ interface. The method of extracting the doping profiles is verified using data from a TCAD simulation of the two MOSFETs. The details of the methods and of the problems encountered are discussed.

Keywords: Silicon pixel sensor, p-type silicon, p-spray, doping profile, MOSFET, TCAD simulations.

Contents

1	Introduction	1
2	MOSFETs investigated and measurement setup	1
3	Data analysis and results	2
3.1	MOSFET parameters extracted from the $I_{ds}(V_{gate})$ measurements	2
3.2	Doping determination: <i>Method 1</i>	5
3.3	Doping determination: <i>Method 2</i>	7
3.4	Comparison to TCAD simulations	11
4	Summary and conclusions	13
5	List of References	15

*Corresponding author. Email address: Robert.Klanner@desy.de, Tel.: +49 40 8998 2558

1. Introduction

In segmented n^+p silicon sensors positive charges in the SiO_2 close to the Si-SiO₂ interface can cause an electron accumulation layer, which essentially shortens the n^+ implants of the electrodes. The positive oxide charges are the result of the growing of the SiO_2 on the Si. Radiation damage due to ionising radiation typically further increases the density of positive oxide charges. A p^+ implantation, either over the entire wafer (p -spray) or as strips (p -stop) or a combination of both is frequently used to isolate the n^+ electrodes [1, 2, 3, 4]. In most cases the implantation dose and the following thermal activation process is not communicated by the vendor. However, the knowledge of the value and of the density profile of active acceptors is required to understand and simulate the performance of the sensors. This is particularly relevant if the sensors are operated in a high radiation field, like at the CERN LHC or the European X-ray Free-Electron Laser, EuXFEL. Therefore, reliable methods for determining the profile of active acceptors are highly desirable. For electronics applications a number of methods, both destructive and non-destructive, are readily available. An overview can be found in Ref. [5]. Given the high resistivity of several $\text{k}\Omega\text{ cm}$ of the silicon used for detector fabrication, the applicability and accuracy of the different methods has to be evaluated.

In this paper we use current-voltage measurements in the linear region of one circular n MOSFET with and a second one without a p -spray implant, to determine the value and the profile of the p -spray implants. In addition, the electron mobilities in the inversion layer at the Si-SiO₂ interface as function of the electric field normal to the interface for the two MOSFETs are determined. The MOSFETs have been fabricated by Hamamatsu [6] on $\sim 4\text{ k}\Omega\text{ cm}$ p -type silicon together with test sensors for the *CMS HPK Campaign* [7, 8, 9] of the CMS Collaboration working at the CERN LHC. For a verification of the method, data from TCAD simulations of the two MOSFETs are analysed with the same software as the experimental data, and input and results compared. The paper presents the problems encountered using the standard methods of the MOSFET analysis developed for electronics and how some of them could be overcome. More information on the measurements and the analysis can be found in [10].

2. MOSFETs investigated and measurement setup

The MOSFETs were fabricated on Magnetic Czochralski p -type silicon with the crystal orientation $\langle 100 \rangle$. Fig. 1a shows a cross section of the circular MOSFET without p -spray implant. The thickness of the Si is approximately $200\ \mu\text{m}$. The Si-bulk dopant density, derived from the $C - V$ measurement of pad diodes is $CN_{bulk} = (3.3 \pm 0.3) 10^{12}\ \text{cm}^{-3}$, where the spread of the measured depletion voltage from different samples and the uncertainty of the effective silicon thickness contribute about equally to the uncertainty. Here and in the following we use CN for the volume dopant concentration with units $[\text{cm}^{-3}]$ and N for the area dopant concentration with units $[\text{cm}^{-2}]$. The maximum dopant densities of the n^+ implants of Source and Drain and of the p^+ back contact are approximately $10^{19}\ \text{cm}^{-3}$, and the junction depths are about $2\ \mu\text{m}$. The oxide thickness, determined using capacitance measurements on MOS capacitors, is $t_{ox} = 700 \pm 5\ \text{nm}$. The metal overlaps of the gate over the n^+ implants are estimated to be about $4\ \mu\text{m}$.

Following the nomenclature of the *CMS HPK Campaign* the MOSFET without p -spray implant is called **M200P**, and the MOSFET with p -spray implant **M200Y**.

Fig. 1b shows the biasing scheme for the MOSFET measurements, which were made on a prober station at approximately 20°C in ambient atmosphere. The Source was put on ground potential. The Drain was biased at $V_{ds} = 50\ \text{mV}$, and the Drain-Source current I_{ds} was measured using a Keithley 6487 PicoAmmeter/Voltage Source. The backside voltage V_{back} was set manually in the range 0 to $-30\ \text{V}$ for the M200P, and from $+0.5\ \text{V}$ to $-30\ \text{V}$ for the M200Y. As the extracted value of the doping concentration is very sensitive to the exact value of V_{back} , this voltage has been recorded with an accuracy at the $1\ \text{mV}$ level, which is more precise than the setting accuracy of the voltage source. For a given value of V_{back} , V_{gate} was ramped from $-6\ \text{V}$ to $+16\ \text{V}$ and I_{ds} recorded. It was verified that the results for ramping V_{gate} up and down are compatible.

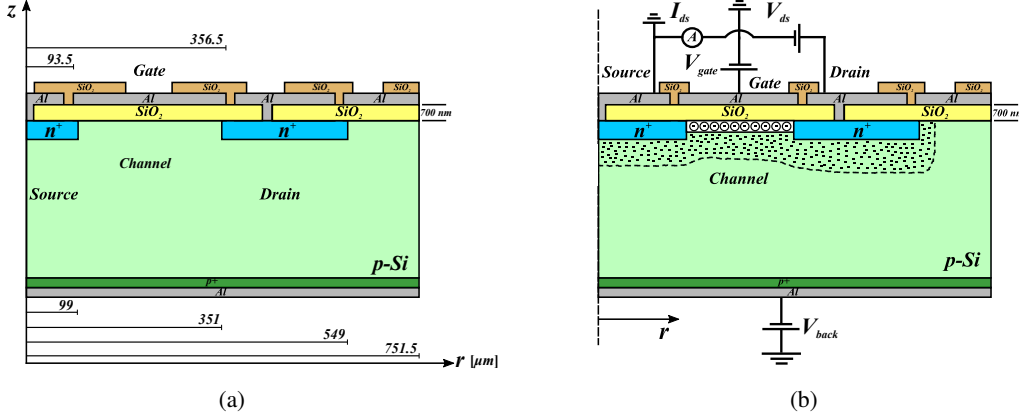


Figure 1: (a) Schematic cross section of the MOSFET. The dimensions are taken from the GDS files of the photomask and (b) measurement setup.

3. Data analysis and results

3.1. MOSFET parameters extracted from the $I_{ds}(V_{gate})$ measurements

Fig. 2 shows a selection of the $I_{ds}(V_{gate}, V_{back})$ results. For the M200Y measurements and $V_{back} > 0.3$ V, the p^+n junctions of Source and Drain approach forward biasing and the diffusion current contributes significantly to I_{ds} . Therefore for these data the I_{ds} current measured at $V_{gate} = -6$ V has been subtracted. Comparing the results of M200Y, the MOSFET with p -spray implant, to the ones of M200P, the MOSFET without p -spray implant, one notices: For $V_{back} \lesssim -2$ V, apart from a shift of V_{gate} by about 7 V, the curves and their spacings with V_{back} are similar, and for $V_{back} \gtrsim -2$ V, the spacings remain approximately constant for M200P, but increase rapidly for M200Y. These differences are caused by the p -spray implant, as will be shown in Sect. 3.2. In addition, the shapes of all curves are similar with the exception of the M200Y measurement at $V_{back} = 0.5$ V. This difference can be described by a change of the electron mobility at the Si-SiO₂ interface.

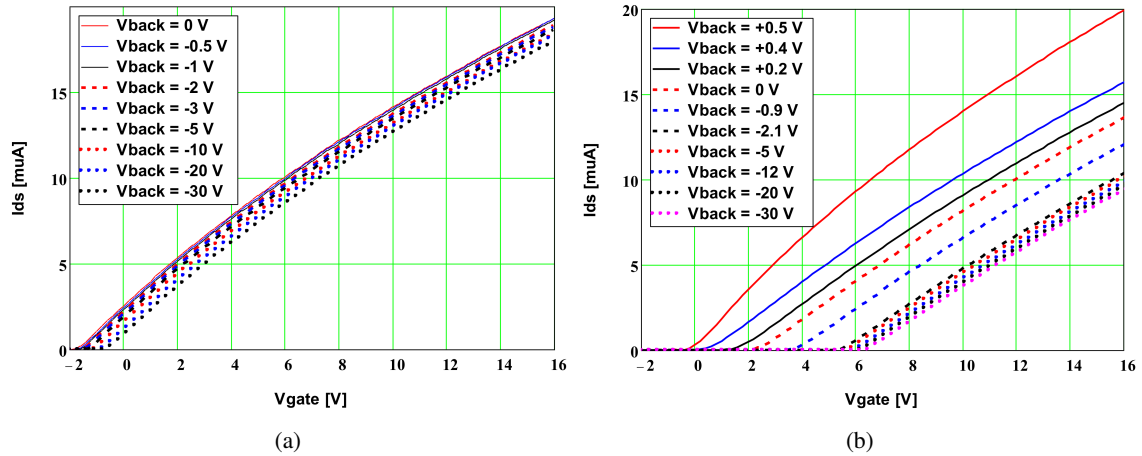


Figure 2: Measured $I_{ds}(V_{gate})$ at $V_{ds} = 50$ mV for the MOSFET (a) M200P and (b) M200Y.

To extract the MOSFET parameters, the standard formula for an n -MOSFET in the linear region, adapted for the circular geometry, is used [11, 12, 13]:

$$I_{ds} \approx \frac{W}{L} \cdot \mu_e \cdot C_{ox} \cdot (V_{gate} - V_{th}) \cdot V_{ds}. \quad (1)$$

The width-over-length ratio for the circular MOSFET is given by $W/L = 2\pi/\ln(r_2/r_1) = 4.964$, with r_1 the outer radius of the Source-implant, and r_2 the inner radius of the Drain-implant. The value of the oxide capacitance $C_{ox} = 4.933 \text{ nF/cm}^2$. The mobility of the electrons is denoted by μ_e , where the following parametrisation of its dependence on V_{gate} and V_{th} has been used [5]:

$$\mu_e = \mu_0 \cdot \frac{1}{1 + \frac{V_{gate} - V_{th}}{V_{1/2}}}, \quad (2)$$

with μ_0 the electron mobility at the Si-SiO₂ interface for $V_{gate} - V_{th} = 0$, and $V_{1/2}$ the value of $V_{gate} - V_{th}$ at which the mobility has decreased by a factor 2 relative to μ_0 , and the threshold voltage V_{th} . The measurements were taken in the linear MOSFET region at $V_{ds} = 50 \text{ mV}$. For $V_{back} = 0$ it has been verified that in the range 25 mV to 200 mV the results do not depend on the choice of V_{ds} [14].

To determine the free parameters of the model, V_{th} , μ_0 and $V_{1/2}$, Eq. 1 was fitted to the data shown in Fig. 2. Figs. 3 and 4 show the dependence on V_{back} of the parameters determined. For M200P the V_{gate} voltage range selected for the fit was $\approx 2.5 \text{ V}$ above V_{th} ; the model describes the data within $\approx 0.2 \%$ and the statistical errors obtained from the fit are $\delta V_{th} \approx 3.5 \text{ mV}$, $\delta \mu_0 \approx 1.5 \text{ cm}^2/\text{V s}$ and $\delta V_{1/2} \approx 0.2 \text{ V}$ if an uncertainty of the I_{ds} measurement of 0.1% is assumed. For M200Y the V_{gate} voltage range selected for the fit was $\approx 5 \text{ V}$ above V_{th} for positive V_{back} values decreasing to $\approx 2.5 \text{ V}$ for the higher negative V_{back} values; the data are described within about 0.05%, and the uncertainties are for δV_{th} between 5 and 10 mV, for $\delta \mu_0 \approx 1.5 \text{ cm}^2/\text{V s}$, and for $\delta V_{1/2} \approx 0.2 \text{ V}$ for an assumed 0.1% I_{ds} uncertainty.

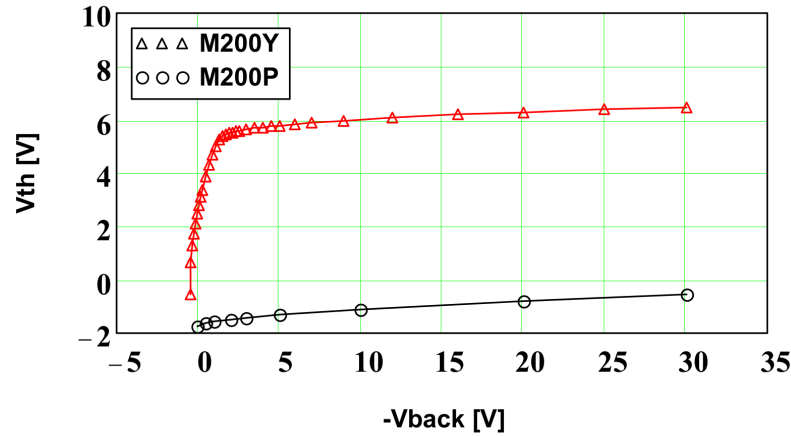


Figure 3: Dependence of the threshold voltage V_{th} on V_{back} for M200P, the MOSFET without p -spray implant and for M200Y, the MOSFET with p -spray implant.

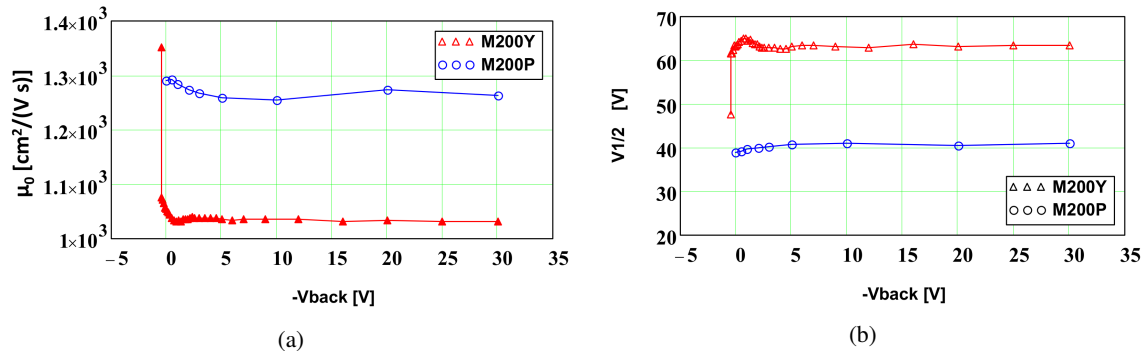


Figure 4: Dependence on V_{back} of (a) μ_0 , the electron mobility in the inversion layer at the threshold voltage V_{th} , and of (b) $V_{1/2}$, the value of $V_{gate} - V_{th}$ at which the mobility has decreased by a factor 2 relative to μ_0 .

Fig. 5 shows the dependence of the mobility on E_S , the electric field in the Si at the Si-SiO₂ interface. Using Gauss's law it can be obtained from the charge density of the inversion layer, $q_0 \cdot N_{inv}$, and the charge per unit area of the depleted silicon, $q_0 \cdot N_{Si}$ (Eq. 14):

$$E_S = \frac{q_0 \cdot (N_{Si} + N_{inv})}{\epsilon_{Si}}. \quad (3)$$

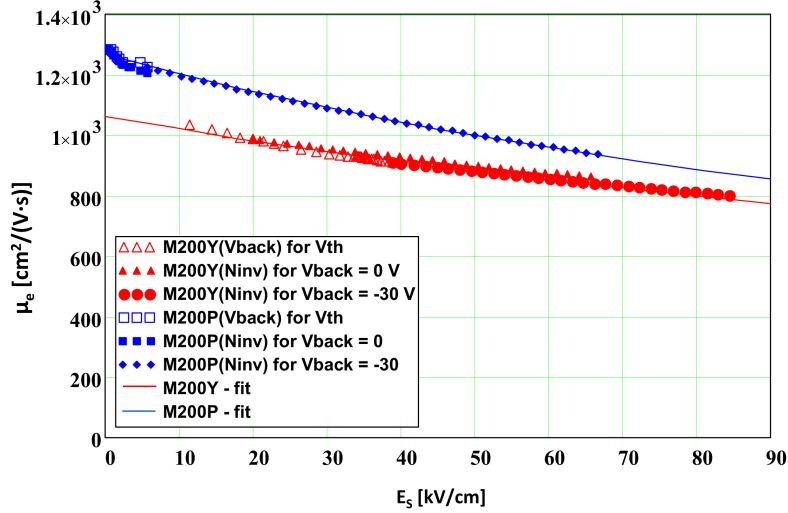


Figure 5: Dependence of the electron mobility in the inversion layer of the MOSFETs with and without p -spray implant as function of the electric field component at the Si-SiO₂ pointing from the SiO₂ to the Si. The points are the measurement results, and the lines the fit by Eq. 4.

In Fig. 5 the results of two different ways of determining the electron mobility, μ_e , are shown: For open symbols the mobility is obtained from $\mu_0 = \mu_e(V_{gate} = V_{th})$ of the $I_{ds}(V_{gate})$ fits for different values of V_{back} , and for the filled symbols the values of μ_e from the fits at the constant V_{back} values of 0 and -30 V. The two methods cover different regions of E_S , but agree within a few percent in the regions of overlap.

For both M200P and M200Y the electron mobility at the Si-SiO₂ interface decreases with electric field. The mobility for the p -spray MOSFET is always lower than for the non- p -spray MOSFET. The reason could be the additional scattering of the electrons on the higher density of dopant atoms, however, the decrease by up to $\approx 15\%$ is larger than the $\approx 5\%$ mobility decrease at a doping of $2 \cdot 10^{15} \text{ cm}^{-3}$ reported in Ref. [15]. Carrier-carrier scattering in the inversion layer [16] also reduces the mobility. In order to make the results available for simulations, the mobility has been fitted by the function

$$\mu_e^E = \frac{\mu_{0,e}^E}{1 + \frac{E_S}{E_{1/2}}}. \quad (4)$$

The results of the fits are shown as lines in Fig. 5, and the parameters obtained in Table 1. The chosen parametrisation provides an adequate description of the measurements.

	$\mu_{0,e}^E$ [cm ² /(V·s)]	$E_{1/2}$ [kV/cm]
M200P (data)	1267 ± 15	190 ± 15
M200P (TCAD)	1498 ± 15	181 ± 15
M200Y (data)	1063 ± 20	240 ± 20
M200Y (TCAD)	1259 ± 40	259 ± 40

Table 1: Parameters obtained by fitting the data of Fig. 5 by Eq. 4, and similar for the TCAD simulations discussed in Sect. 3.4.

3.2. Doping determination: Method 1

In this section a simplified analysis is used to determine the bulk doping, CN_{bulk} , the integrated p -spray dose, N_{imp} , and an estimate of the maximal p -spray dopant density, CN_{imp} . Here and in the following we call CN the dopant density with units cm^{-3} , and its integral with N and units cm^{-2} . The method used is simpler than the way the dopant profile is determined in Sect. 3.3 and less affected by measurement errors, as it does not require a differentiation of experimental measurements. However, assumptions have to be made on the surface potential, Φ_S , and its validity is limited to regions of constant doping density.

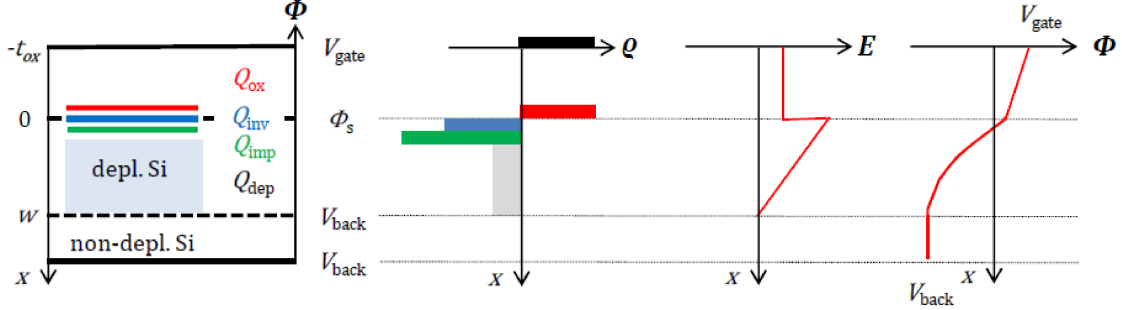


Figure 6: Schematic representation of the location of charges in a MOSFET in inversion conditions, and qualitative dependence of the charge density, ρ , transverse electric field, E , in the Si at the Si-SiO₂ interface and electric potential Φ . For the charge densities Q_{imp} , Q_{inv} and Q_{ox} δ function distributions at $x = 0$ are assumed for the sketch of E and Φ .

The method is explained with the help of Fig. 6. From the measurements we know V_{back} , V_{gate} and I_{ds} . From the physics of MOS structures we know that the potential at the interface at inversion $\Phi_S \approx 2\psi_B + f_{ds} \cdot V_{ds}$, where $\psi_B = \frac{k_B T}{q_0} \cdot \ln(CN_A/n_i)$ is the distance of the Fermi level from the middle of the band gap. The doping density at the Si-SiO₂ is denoted CN_A , the Boltzmann constant, k_B , the absolute temperature T , and the intrinsic charge carrier density at room temperature $n_i \approx 10^{10} \text{cm}^{-3}$. The term $f_{ds} \cdot V_{ds}$ is the difference of the average potential of the conducting channel of the MOSFET to the potential at the n^+p junction of the source. For a linear MOSFET $f_{ds} = 0.5$, and for a circular MOSFET, where the potential depends on the logarithm of the radius, $f_{ds} = 0.691$. The oxide charge density, $Q_{ox} = q_0 \cdot N_{ox}$, can be estimated by extrapolating V_{th} , shown in Fig. 3, to $V_{back} = \Phi_S$, and using the relation $Q_{ox} = C_{ox} \cdot [V_{th}(V_{back} = \Phi_S) - \Phi_S]$. These relations can be understood in the following way: For the threshold condition $Q_{inv} = 0$, and for $V_{back} = \Phi_S$, $Q_{Si} = Q_{dep} + Q_{imp} = 0$. Thus Q_{ox} is the only relevant charge density in the MOSFET, and the biasing of the MOSFET just corresponds to a SiO₂ capacitor of thickness t_{ox} charged to a charge density Q_{ox} . For both M200P and M200Y a value of $N_{ox} \approx 5 \cdot 10^{10} \text{cm}^{-2}$ is found.

From I_{ds} and the electron mobility μ_e , determined using Eq. 2, the charge density of the inversion layer

$$Q_{inv} = -q_0 \cdot N_{inv} = -\frac{L}{W} \cdot \frac{I_{ds}}{\mu_e(V_{gate}, V_{back}) \cdot V_{ds}} \quad (5)$$

is obtained. The negative sign takes into account that electrons make up the inversion layer in p -type Si. Assuming an implantation depth, which is so narrow that it can be approximated by a charge sheet at $x = 0$, and a uniform doping $CN_A(x) = CN_{bulk}$ in the Si, and taking into account that $E_{Si}(w) = 0$, the electric field in the Si bulk is

$$E_{Si}(x) = -\int_w^x \frac{q_0 \cdot CN_A(\xi)}{\epsilon_{Si}} d\xi = \frac{q_0 \cdot CN_{bulk}}{\epsilon_{Si}} (w - x), \quad (6)$$

and the potential

$$\Phi_{Si}(x) = V_{back} - \int_{-w}^x E_{Si}(\xi) d\xi = V_{back} + \frac{q_0 \cdot CN_{bulk}}{2 \epsilon_{Si}} (x - w)^2. \quad (7)$$

From $\Phi_{Si}(0) = \Phi_S$ follows

$$w = \sqrt{\frac{2 \epsilon_{Si}}{q_0 \cdot CN_{bulk}} (\Phi_S - V_{back})} \quad \text{and} \quad E_{Si}(0) = \sqrt{\frac{2 q_0 \cdot CN_{bulk}}{\epsilon_{Si}} (\Phi_S - V_{back})}. \quad (8)$$

Taking into account the charge densities Q_{imp} , Q_{inv} , which are negative, the positive oxide charge density Q_{ox} , and the boundary conditions at the Si-SiO₂ interface, we obtain the relation between V_{gate} and V_{back}

$$V_{gate} = \Phi_S + E_{ox} \cdot t_{ox} = \Phi_S + (\sqrt{2 \varepsilon_{Si} \cdot CN_{bulk}(\Phi_S - V_{back})}/q_0 + N_{imp} + N_{inv} - N_{ox}) \cdot q_0/C_{ox}. \quad (9)$$

Thus for regions of uniform doping, a linear relationship for V_{gate} versus $\sqrt{2 \Phi_S - V_{back}}$ is expected with the slope $\sqrt{2 \varepsilon_{Si} \cdot CN_{bulk} \cdot q_0}/C_{ox}$ and the intercept $\Phi_S + (N_{imp} + N_{inv} - N_{ox}) \cdot q_0/C_{ox}$.

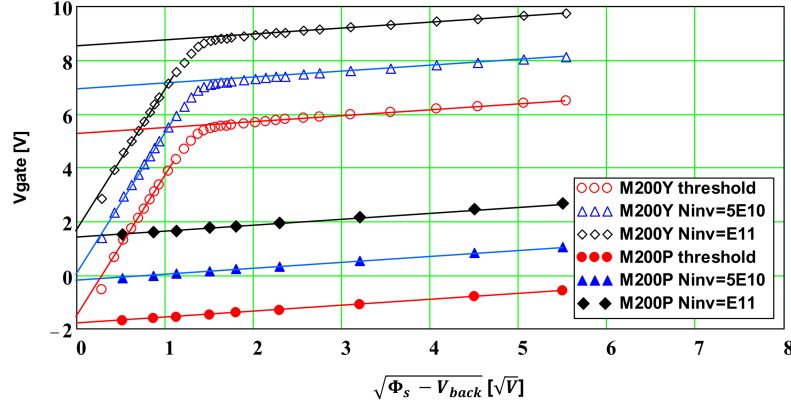


Figure 7: V_{gate} as function of $\sqrt{2 \Phi_S - V_{back}}$ for different N_{inv} values for the MOSFETs M200P and M200Y.

Fig. 7 shows as examples the results for $N_{inv} = 0, 5 \cdot 10^{10} \text{ cm}^{-2}$, and 10^{11} cm^{-2} . For $N_{inv} = 0$ the value of V_{th} has been used for V_{gate} , and for $N_{inv} > 0$ a linear interpolation of V_{gate} between the two closest N_{inv} values using Eq. 5. Table 2 presents the MOSFET doping parameters extracted by this analysis.

For M200P straight lines are observed for all values of N_{inv} , from which we conclude that the doping density is uniform throughout the silicon. As expected, the curves are shifted by steps of $q_0 \cdot N_{inv}/C_{ox} = 1.63 \text{ V}$ for the chosen N_{inv} steps of $5 \cdot 10^{10} \text{ cm}^{-3}$. Using Eq. 9, from the slope a value of the doping of $CN_{bulk} = (3.81 \pm 0.15) \cdot 10^{12} \text{ cm}^{-3}$ is obtained.

For M200Y two linear regions are observed, which is the result of the p -spray doping. As function of N_{inv} , the curves are shifted by the same amount as the M200P curves. From the value of the slope, a bulk doping of $CN_{bulk} = (3.69 \pm 0.15) \cdot 10^{12} \text{ cm}^{-3}$ is obtained, which is similar to the value from the M200P and the bulk doping from $C - V$ measurements of pad diodes reported in Sect. 2. The second linear region at low V_{back} voltages has a slope, which corresponds to a p -implant doping density $CN_{imp} = (1.9 \pm 0.15) \cdot 10^{15} \text{ cm}^{-3}$. Using Eq. 9, the integrated p -spray implant of $N_{imp} = (2.17 \pm 0.05) \cdot 10^{11} \text{ cm}^{-2}$ is derived from the differences of the intercepts of the straight lines for high and low V_{back} voltages. The ratio $N_{imp}/CN_{imp} = (1.14 \pm 0.12) \mu\text{m}$ yields an estimate of the implantation depth.

	Φ_S [V]	CN_{bulk} [cm^{-3}]	CN_{imp} [cm^{-3}]	N_{imp} [cm^{-2}]
M200P	0.33	$(3.81 \pm 0.15) \cdot 10^{12}$	–	–
M200Y	0.65	$(3.69 \pm 0.15) \cdot 10^{12}$	$(1.9 \pm 0.2) \cdot 10^{15}$	$(2.17 \pm 0.05) \cdot 10^{11}$

Table 2: Parameters obtained for the bulk and the p -implant doping for M200P and M200Y.

The analysis presented is quite similar to methods used for the analysis of the doping profiles in MOSFETs for electronics [5]: the *Threshold Voltage Method* [17], which corresponds to the analysis with $N_{inv} = 0$, and the *Constant Drain-Source Current Method* [18, 19], which uses the dependence of V_{gate} on V_{bulk} for constant I_{ds} . We found it necessary to correct I_{ds} for the change in mobility with electric field, in order to have a constant N_{inv} . Fig. 8 compares the results for CN_{bulk} for M200P and M200Y and for CN_{imp} using the requirements of constant N_{inv} to constant I_{ds} in the analysis. Whereas for the constant N_{inv} requirement the extracted doping is constant within a few percent for N_{inv} values between 0 and $4 \cdot 10^{11} \text{ cm}^{-2}$, the constant I_{ds} requirement results in a systematic increase. We conclude that for the determination of the doping densities from MOSFETs on high-ohmic Si the *Constant N_{inv} Method* should be used instead of the *Constant Current Method*.

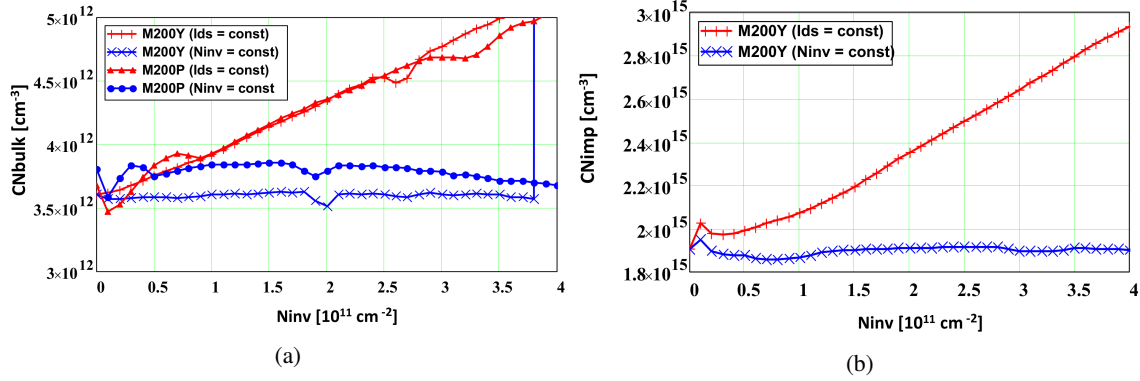


Figure 8: Values of the doping density determined from the straight-line fits to the data as shown in Fig. 7 as function of N_{inv} assuming constant I_{ds} or constant N_{inv} (a) for the bulk doping, CN_{bulk} , of M200P and M200Y, and (b) for the p -spray doping, CN_{imp} , of M200Y.

3.3. Doping determination: Method 2

In this section an attempt is made to determine the doping profiles as well as the integrals of the doping profile of the M200Y and M200P MOSFETs. We first note that, like for the $C - V$ method used for doping-profile determinations, also for MOSFETs the majority carrier concentration, $p(x)$, (holes for an n -MOSFET), and not the doping profile, $CN(x)$ is determined. If $CN(x)$ changes rapidly compared to the Debye length $L_D = \sqrt{(\epsilon_{Si} \cdot k_B \cdot T)/(q_0^2 \cdot CN)}$, the diffusion of holes causes a difference between $CN(x)$ and $p(x)$ [20, 18, 21, 22]:

$$CN(x) = p(x) - \frac{\epsilon_{Si} \cdot k_B \cdot T}{q_0^2} \cdot \frac{d^2 \ln(p(x))}{dx^2}. \quad (10)$$

For a doping $CN = 10^{13} \text{ cm}^{-3}$ the Debye length $L_D = 1.3 \mu\text{m}$ at room temperature, and the difference between the doping profile and the majority-charge carrier distribution, the *Debye correction*, can be significant.

Eq. 10 can be derived under the assumption that the influence of minority charge carriers can be ignored. In this case Gauss's law reads

$$\frac{dE_{Si}(x)}{dx} = \frac{q_0}{\epsilon_{Si}} \cdot (p(x) - CN(x)), \quad (11)$$

and the steady-state current-continuity equation for zero current flow is:

$$j(x) = q_0 \cdot \left(D_h \cdot \frac{dp(x)}{dx} - p(x) \cdot \mu_h \cdot E(x) \right) = 0, \quad (12)$$

with the hole mobility μ_h and the hole diffusion constant $D_h = \mu_h \cdot (k_B \cdot T)/q_0$. Inserting the derivative of Eq. 12 into Eq. 11 results in Eq. 10.

In Refs. [18, 19] the following formulae for the majority-charge carrier density $p(x)$ as function of the distance x from the Si-SiO₂ for a MOSFET with arbitrary doping distribution $CN(x)$ are derived

$$x = \frac{\epsilon_{Si}}{C_{ox}} \cdot \frac{dV_{back}}{dV_{gate}} \quad \text{and} \quad p(x) = \frac{C_{ox}^2}{q_0 \cdot \epsilon_{Si}} \cdot \left(\frac{d^2 V_{back}}{dV_{gate}^2} \right)^{-1}, \quad (13)$$

where $x = w(V_{back}, N_{inv})^1$ is the depletion depth for a given value of V_{back} and N_{inv} , and the values of V_{gate} are obtained by interpolating the $I_{ds}(V_{gate}, V_{back})$ measurements for a given N_{inv} value using

¹This equality follows from the depletion approximation, which states that the charge density is probed at the edge of the depletion region. For the determination of doping profiles using $C - V$ measurements, the corresponding relation is $x = w = \epsilon_{Si}/C_{ox}$

Eq. 5. Anticipating that the second derivatives from the experimental data have large uncertainties and that the Debye correction to the integral of the dopant density, N_{Si} , is small compared to the measurement uncertainties, we also give the formula for the integral of $p(x)$ over the interval x_0 to x , which we call N_{Si}^*

$$\int_{x_0}^x p(x) dx = \frac{C_{ox}}{q_0} \cdot (V_{gate}(x) - V_{gate}(x_0)) \approx N_{Si}^*(x, x_0). \quad (14)$$

This equation, which can be derived from Eq. 13, directly follows from charge neutrality for the entire MOSFET. We note that N_{Si}^* includes both p -spray implant and bulk-dopant densities (see also Fig. 6).

Fig. 9 shows for the MOSFETs M200P and M200Y the depletion depth $w(V_{back})$ for the threshold voltage, and for $N_{inv} = 5 \cdot 10^{10} \text{ cm}^{-2}$ and 10^{11} cm^{-2} . For the derivative dV_{back}/dV_{gate} in Eq. 13, a second order polynomial is put through the V_{back} points below, at and above the corresponding V_{gate} value. For the derivative of the first and last V_{gate} value, the selected V_{gate} points are shifted up and down by one, respectively. Using second order polynomial fits through 5 points or smoothing of the measured points gives compatible results.

For M200P a square root dependence of $w(|V_{back}|)$ is observed, as expected for a uniform doping. For M200Y the change of doping for small values of $-V_{back}$ is much weaker, because of the p -spray implant. This is apparent from Fig. 9b, where the y -axis for the M200P is scaled by a factor 10 compared to M200Y.

Fig. 10 shows the dependence of w on $V_{gate} - (q_0 \cdot N_{inv})/C_{ox}$ for a limited w range. For $w = 0$ the Si is non depleted and acts like a conductor connected to the gate by the capacitance C_{ox} , which is charged up by the oxide-charge density $q_0 \cdot N_{ox}$. For M200P, with its uniform doping density, the potential in the Si is constant and $\Phi_S \approx V_{back}$ and $|V_{gate} - V_{back}| \approx q_0 \cdot N_{ox}/C_{ox}$. Therefore, extrapolating the $w(V_{back})$ and $w(V_{gate} - (q_0 \cdot N_{inv})/C_{ox})$ curves to $w = 0$ allows to determine Φ_S and N_{ox} . The results are shown in Table 3. For M200Y, the doping is very nonuniform due to the p -spray implant, the potential in the Si depends on x , even for $w = 0$, and the situation is significantly more complicated.

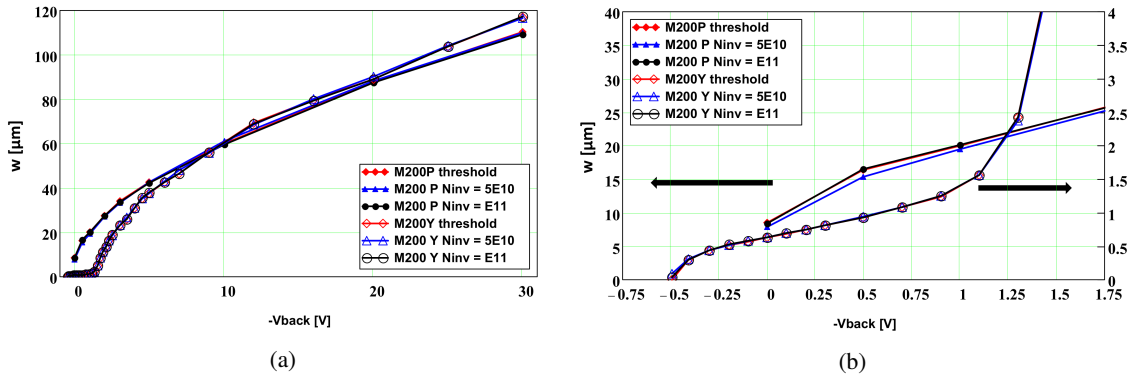


Figure 9: Depletion depth w as function of $-V_{back}$ for M200P and M200Y for the threshold voltage, for $N_{inv} = 5 \cdot 10^{10} \text{ cm}^{-2}$ and 10^{11} cm^{-2} , for (a) the entire, and (b) the $-V_{back}$ range between -0.75 and 1.75 V. As discussed in the text, the extrapolation to $w = 0$ allows to estimate the potential at the interface Φ_S . Note that in (b) the y scale for M200Y is expanded by a factor 10.

	$V_{back}(w = 0)$ [mV]	$V_{gate}(w = 0)$ [V]	N_{ox} [cm^{-2}]
M200P (data)	150 ± 80	-1.82 ± 0.10	$(6.0 \pm 0.3)10^{10}$
M200P (TCAD)	350 ± 80	$-2.0^{+1.0}_{-0.5}$	$(6.2^{+3.0}_{-1.5})10^{10}$
M200Y (data)	510 ± 25	-0.61 ± 0.05	–
M200Y (TCAD)	800^{+500}_{-250}	-2.0 ± 1.0	–

Table 3: Values of V_{back} and V_{gate} for zero depletion depth, w for the experimental data and the data simulated with TCAD discussed in Sect. 3.4.

Fig. 11 shows $N_{Si}^*(x, 0)$, the integral over the free charge carrier density $p(x)$ between zero depletion width, $w = x = 0$ and x , which to a good approximation is equal to the integral of the dopant density from

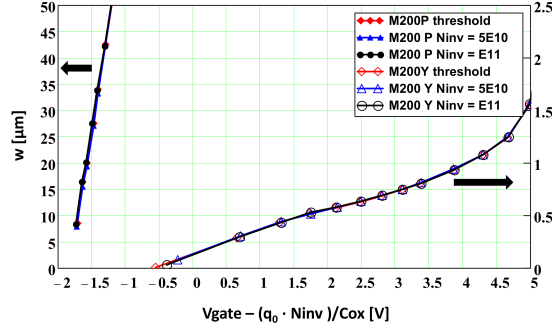


Figure 10: Depletion depth w as function of $V_{gate} - (q_0 \cdot N_{inv}) / C_{ox}$ for M200P and M200Y for the threshold voltage, corresponding to $N_{inv} = 0$, for $N_{inv} = 5 \cdot 10^{10} \text{ cm}^{-2}$ and 10^{11} cm^{-2} . As discussed in the text, the extrapolation to $w = 0$ allows to estimate the oxide-charge density N_{ox} . Note that the y scale for M200Y is expanded by a factor 20.

the Si-SiO₂ interface to x (see Fig. 6). The values obtained for the three values of N_{inv} presented in the figure, zero for V_{th} , $5 \cdot 10^{10} \text{ cm}^{-2}$ and 10^{11} cm^{-2} are on top of each other in the figure and thus agree. The agreement for the other N_{inv} values, which are not shown, is similar. For $x \gtrsim 10 \mu\text{m}$ the slope of the linear increase of $N_{Si}^*(x)$ is the same within 1% for M200P and M200Y, from which we conclude that they have the same constant bulk doping. For $x \lesssim 2 \mu\text{m}$ the M200Y data show a rapid increase, which reflects the p -spray implant.

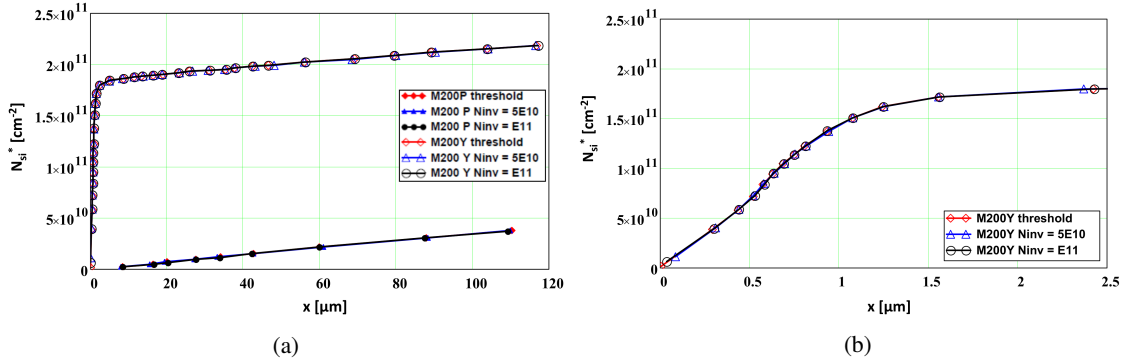


Figure 11: Approximate dopant density N_{Si}^* as function of x , the distance from the Si-SiO₂ interface for M200P and M200Y for the threshold voltage, $N_{inv} = 5 \cdot 10^{10} \text{ cm}^{-2}$ and 10^{11} cm^{-2} , for (a) the entire studied x range, and (b) the x range up to $2.5 \mu\text{m}$.

In order to estimate the density of free charge carriers, $p(x)$, $N_{Si}^*(x, x_0)$ is differentiated with respect to x . The results are shown in Fig. 12. It can be seen that, in particular around the maximum of $p(x)$, major differences for the three N_{inv} values shown are observed. The reason is that the values of $p(x)$ are very sensitive to the exact values of V_{gate} , which are obtained by interpolating the $I_{ds}(V_{gate})$ results, and of V_{back} , which has been recorded with an accuracy of $\approx 1 \text{ mV}$, significantly more precise than the setting uncertainty of the Keithley 6487. In order to obtain a smooth result, the individual values of V_{back} had to be changed manually by up to $\pm 2 \text{ mV}$ in the analysis. The change of a single V_{back} value by 2 mV in the region of the maximum of $p(x)$, results in an S-shaped deviation with an amplitude of $\approx 30\%$. Thus the determination of $p(x)$ can only be considered an estimate, however the integral $N_{Si}^*(x, 0)$ is a reliable determination. Its uncertainty is given by the uncertainty of determining the value of $x = 0$. We note that for understanding the effect of the p -spray doping on the isolation and resistance between n^+ implants on p -Si, the integral $N_{Si}^*(x, 0)$ is the relevant quantity. Nevertheless, in order to provide a doping profile, which can be used in TCAD simulations, and to estimate the size of the Debye correction, $p(x)$ has been fitted by

the phenomenological function

$$p(x) = A \cdot \exp\left(\frac{-(x - \mu)^2}{2 \cdot (\sigma_0^2 + \sigma_1^2 \cdot (x - \mu)^2)}\right) + B, \quad (15)$$

which is a Gaussian function with a width, which increases with the distance from the mean value μ , and finally approaches a constant plus the constant B . The function only approximately describes the observed $p(x)$ dependence and deviations of up to 20% are observed. The best description is obtained for low N_{inv} values and in Fig. 13 data and fit for $N_{inv} = 10^{10} \text{ cm}^{-2}$ are shown. The Debye correction (Eq. 10) amounts to +5% at the maximum of $p(x)$, and to -20% at $x = 3 \mu\text{m}$, and thus is similar to the uncertainties of the measurement results. Although this is only a crude estimate, it is clear that the Debye correction does not explain the non-Gaussian tails of $p(x)$. The parameters from the fit are given in Table 4. For large x values the constant bulk doping of $A \cdot \exp(-0.5/\sigma_1^2) + B = 3.8 \cdot 10^{12} \text{ cm}^{-3}$ is obtained.

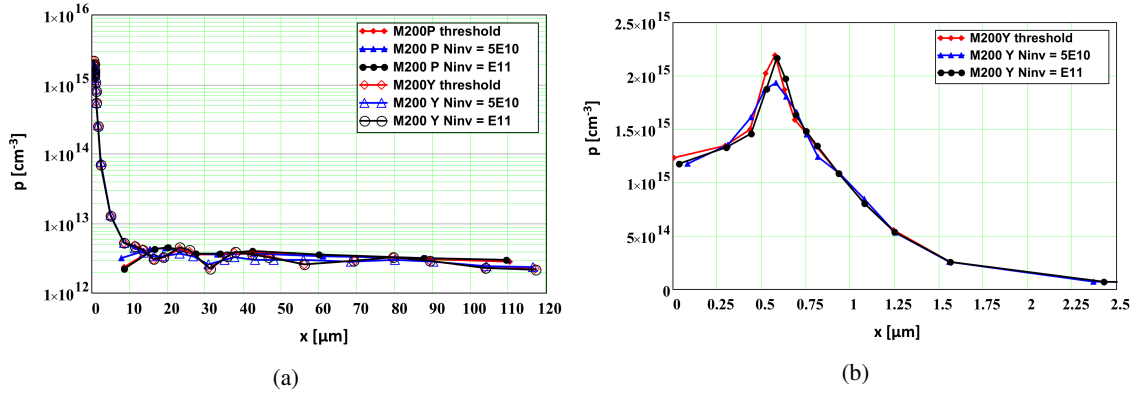


Figure 12: Free charge carrier density p as function of x , the distance from the Si-SiO₂ interface for M200P and M200Y for the threshold voltage, $N_{inv} = 5 \cdot 10^{10} \text{ cm}^{-2}$ and 10^{11} cm^{-2} , for (a) the entire x range studied, and (b) the x range up to $2.5 \mu\text{m}$.

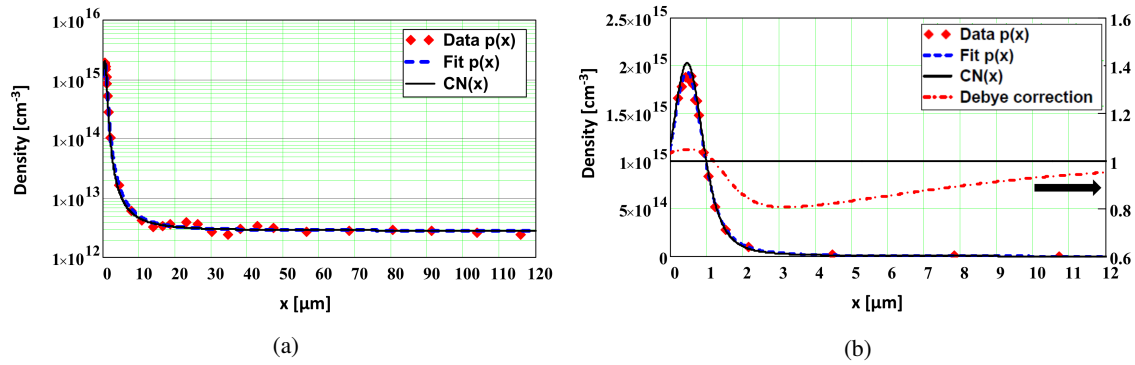


Figure 13: Free charge carrier density $p(x)$, fit by Eq. 15 and doping density after the Debye correction, $CN(x)$, as function of x , for M200Y for $N_{inv} = 10^{10} \text{ cm}^{-2}$ for (a) the entire studied x range, and (b) the x range up to $12 \mu\text{m}$; the right y scale refers to the ratio of the Debye correction to $p(x)$.

$A [\text{cm}^{-3}]$	$B [\text{cm}^{-3}]$	$\mu [\mu\text{m}]$	$\sigma_0 [\mu\text{m}]$	σ_1
$1.96 \cdot 10^{15}$	$-2.93 \cdot 10^{13}$	0.462	0.418	0.350

Table 4: Parameters of the fit of Eq. 15 to the data of Fig. 11. The function describes the data with an estimated uncertainty of $\approx 20\%$.

3.4. Comparison to TCAD simulations

To verify the analysis methods used to extract the MOSFET parameters, in particular the doping profile close to the Si-SiO₂ interface, simulations using SYNOPSIS TCAD [23] were performed. The MOSFET geometry used for the simulation is given in Fig 1a. For the M200P a constant p -doping density of $3.5 \cdot 10^{12} \text{ cm}^{-3}$ and for M200Y the p doping profile derived from the measurements in Sect. 3.3 with the values given in Table 4, are assumed. They correspond to a maximal p^+ doping of $2 \cdot 10^{15} \text{ cm}^{-3}$ at a distance of $0.46 \mu\text{m}$ from the Si-SiO₂ interface, and a bulk doping of $3.8 \cdot 10^{12} \text{ cm}^{-3}$. The back contact is simulated by an p^+ implant with a maximal doping density of 10^{19} cm^{-3} and a depth of $2 \mu\text{m}$. For the oxide charge density a value of $5 \cdot 10^{10} \text{ cm}^{-2}$ is assumed for both MOSFETs. For the doping dependence of the electron mobility the model of Masetti [24] with the transverse electric field dependence of Lombardi [15] and the carrier-carrier scattering model of Conwell-Weisskopf [16], are used.

For the M200Y the grid has 356 000 points and 709 000 elements, with grid spacings in the Si close to the Si-SiO₂ interface of 0.2 nm, 0.8 nm, 0.8 nm and further spacings of 1.4 nm. Such small spacings are required for a realistic simulation of the inversion layer. Fig. 14 shows the layout, the grid and the doping distribution of the M200Y in the region of the corner of the source n^+ implant implemented for the simulation. The simulation of the complete data set for the M200Y takes 35 hours on 16 Intel XENON ES-2640v3 CPUs operating at 2.6 GHz. The requirements for the simulation of the M200P is significantly less challenging and time consuming. We note that, apart from the circular geometry, the basic structure of the M200Y is very similar to a segmented n^+p sensor, and we find that a fine grid close to the Si-SiO₂ interface is required for obtaining reliable results.

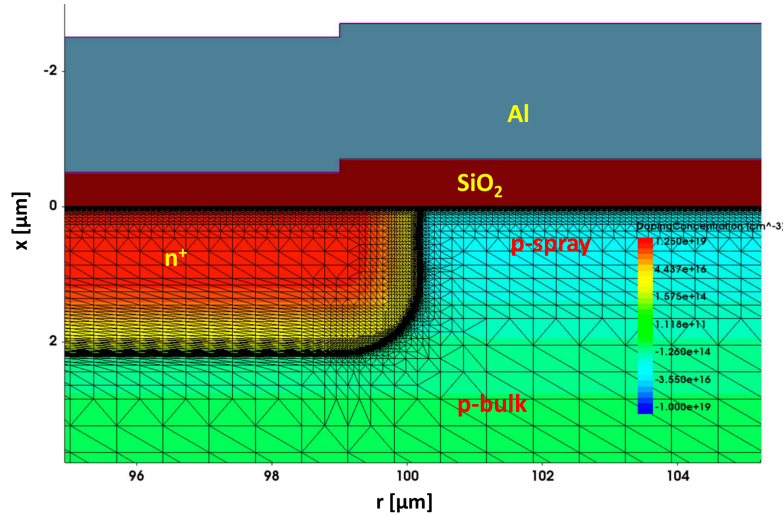


Figure 14: Grid and doping distribution implemented in the TCAD simulation for the MOSFET M200Y at the corner of the source n^+ implant. The distance from the center of the circular MOSFET is denoted by r .

In the following, we present and discuss some of the results of the analysis of the data from the TCAD simulation. The dependence of I_{ds} on V_{gate} for the different values of V_{back} of the simulated data is very similar to the experimental data shown in Fig. 2. An exception are the results for M200Y for $V_{back} = 0.5$: The $V_{back} = 0.5$ curve is closer to the $V_{back} = 0.4$ V curve for the simulation than for the experimental data. The fits of Eqs. 1 and 2 to $I_{ds}(V_{gate})$, which are used to determine the free parameters of the model, are of similar quality as for the experimental data, with deviations between fit results and data at the 0.1 % level.

Fig. 15 shows the dependence of V_{th} on V_{back} derived from the TCAD data. When compared to the experimental data of Fig. 3, only minor differences are observed. Fig. 16 shows the dependence of the electron mobility μ_e on the electric field at the Si-SiO₂ interface, E_S , derived from the TCAD data, to be compared to Fig. 5 for the experimental data. Here, major differences are observed. For both M200P and M200Y the mobility values from the simulation are significantly higher. For M200Y the mismatch of the mobility determined from the $V_{back} = 0$ V and the -30 V simulations, is larger than for the experimental data. Table 1 gives the parameters of the fit of Eq. 4 to the simulated data, which is shown as solid line

in the figure. In spite of significant differences between experimental and simulated values, we have not implemented the experimentally determined mobility parametrisation into the TCAD simulation, as the value of the mobility should not influence the determination of the doping profile, which is the main aim of the paper.

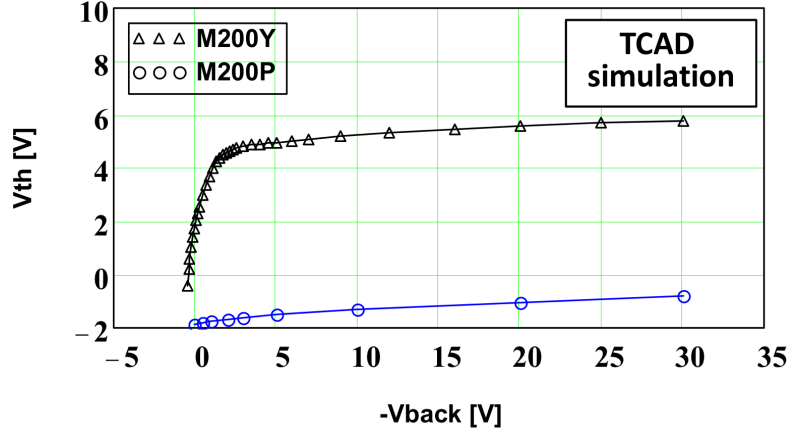


Figure 15: Dependence of the threshold voltage V_{th} on V_{back} derived from the TCAD data for the M200P and the M200Y MOSFETs.

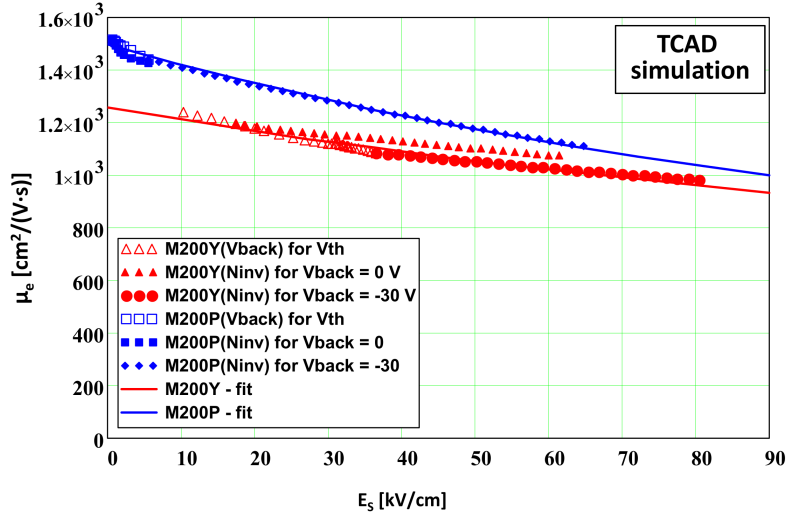


Figure 16: Dependence of the electron mobility in the inversion layer on the electric field component normal to the Si-SiO₂ interface derived from the TCAD data for the M200P and the M200Y MOSFETs. The points are the simulation results, and the lines the fit by Eq. 4.

Using *Method 1* of Sect. 3.2, which assumes regions of constant doping density and the knowledge of the potential at the Si-SiO₂ interface, Φ_S , the bulk doping, CN_{bulk} , and the maximum and integral of the p -spray doping, CN_{imp} and N_{imp} , have been extracted from the simulated data. In Table 5 the results are compared to the input values of the simulation. For the M200P MOSFET the values for the bulk doping, which is constant, agree. For the M200Y MOSFET the extracted bulk doping is 20% higher than the input value, where we note that the extracted value depends on range of V_{back} used in the analysis: For the range -5 V to -30 V the value is $CN_{bulk} = 4.75 \cdot 10^{12} \text{ cm}^{-3}$, whereas for the range -20 V to -30 V $CN_{bulk} = 4.15 \cdot 10^{12} \text{ cm}^{-3}$. As expected, the values for the integrated dose, N_{imp} , which is the relevant parameter for understanding the isolation of p implants and which is determined with an accuracy of $\approx 5\%$, agree. The maximum of the p -implant doping, N_{imp} , and the effective implantation depth, $d_{imp} = N_{imp}/CN_{imp}$, also agree within their significantly larger uncertainties.

	CN_{bulk} [cm ⁻³]	CN_{imp} [cm ⁻³]	N_{imp} [cm ⁻²]	d_{imp} [μm]
M200P (input)	$3.5 \cdot 10^{12}$	–	–	–
M200P (results)	$(3.5 \pm 0.1) \cdot 10^{12}$	–	–	–
M200Y (input)	$3.8 \cdot 10^{12}$	$1.93 \cdot 10^{15}$	$2.1 \cdot 10^{11}$	1.09
M200Y (results)	$(4.3 \pm 0.5) \cdot 10^{12}$	$(1.6 \pm 0.3) \cdot 10^{15}$	$(2.0 \pm 0.1) \cdot 10^{11}$	1.25 ± 0.20

Table 5: Comparison of the input data to the analysis results using *Method 1* for the TCAD simulations.

The further analysis of the simulated data follows *Method 2* of Sect. 3.3. Using Eq. 13 the depletion depth, w , is determined for constant values of the charge density of the inversion layer, N_{inv} . The results on the dependence of w on V_{back} and on $V_{gate} - (q_0 \cdot N_{inv})/C_{ox}$ are shown in Fig. 17 for three values of N_{inv} . It can be seen that the results are independent of N_{inv} : Except for the $V_{back} = 0.5$ V results for M200Y, the different N_{inv} points are on top of each other. Comparing to the experimental data, which are shown in Figs. 9 and 10, the shape of the curves for both M200P and M200Y are compatible, but the M200Y curve is shifted by $\approx +0.5 \mu\text{m}$ and the M200P curve by $\approx +2 \mu\text{m}$ relative to the experimental curves. We do not understand the reason for this difference. The values for V_{back} and of V_{gate} extrapolated to $w = 0$ are reported in Table 3. Because of the larger extrapolation in w , the uncertainties for the simulated data are larger than for the experimental data. Within their uncertainties the results are compatible.

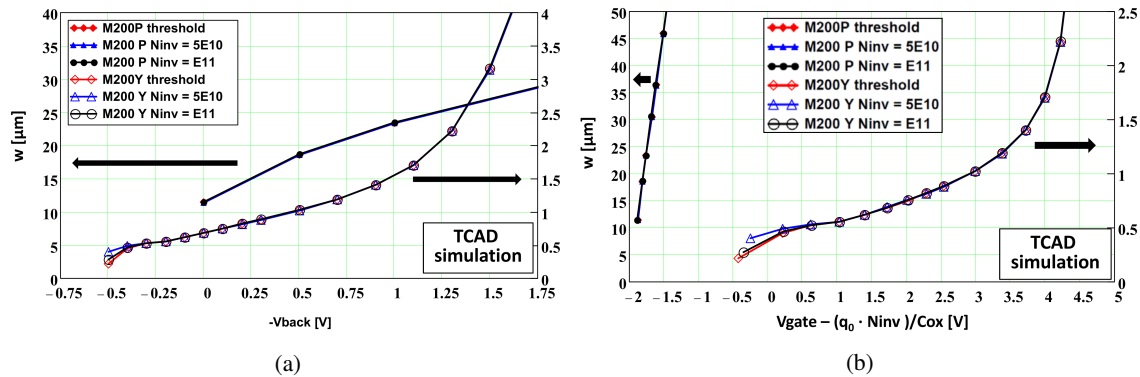


Figure 17: Depletion depth w as function of (a) $-V_{back}$, and (b) of $V_{gate} - (q_0 \cdot N_{inv})/C_{ox}$ for M200P and M200Y for the threshold voltage, for $N_{inv} = 5 \cdot 10^{10} \text{ cm}^{-2}$ and 10^{11} cm^{-2} , for the analysis of the simulated data. Note that in the y scale on the right side for M200Y is expanded by a factor 10 for (a) and by a factor 20 for (b).

The majority charge carrier density, $p(x)$, is obtained by differentiating N_{Si}^* from Eq. 14 with respect to x from Eq. 13. In Fig. 18 the results are compared to the input doping profiles: $3.5 \cdot 10^{12} \text{ cm}^{-3}$ for M200P, and the function given in Eq. 15 with the parameters from Table 4 for M200Y. It is found that the results do not depend on N_{inv} , and only the values for $N_{inv} = 5 \cdot 10^{10} \text{ cm}^{-2}$ are shown. For $x \geq 0.5 \mu\text{m}$ the reconstructed and input values agree within $\leq 10\%$. The values for $x \leq 0.5 \mu\text{m}$ show big fluctuations, which appear unphysical and are not described by the smooth parametrisation. Investigating the simulated charge density and field distributions reveals large fluctuations in this region, which may cause the fluctuations in the results. We also note that for the simulation the integrated p -spray dose is $\approx 5\%$ higher than the input value.

In spite of these differences, we consider the agreement between analysis results and input data satisfactory, and conclude that the proposed method of determining doping profiles using MOSFETs on high-ohmic silicon is valid.

4. Summary and conclusions

In this paper an attempt is made to determine the doping profile of the p -spray implant, which is used to electrically isolate n^+ implants in segmented n^+p silicon sensors. For circular MOSFETs with and without p -spray implant, produced as test structures together with silicon sensors, the Drain-Source current, I_{ds} ,

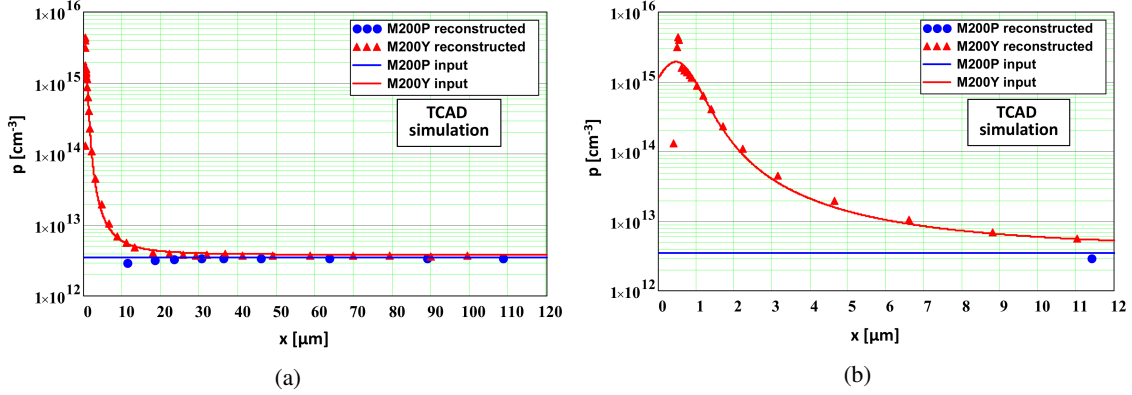


Figure 18: Comparison of the input to the reconstructed free charge carrier density p as function of x , the distance from the Si-SiO₂ interface for the simulated M200P and M200Y data, where $N_{inv} = 5 \cdot 10^{10} \text{ cm}^{-2}$ has been selected; (a) the entire x range studied, and (b) the x range up to 12 μm .

has been measured as function of the gate voltage, V_{gate} , for different values of the back-side voltage, V_{back} . The measurements were performed at room temperature and ambient atmosphere in the linear MOSFET region for a Drain-Source voltage $V_{ds} = 50 \text{ mV}$ on a standard chuck. The value of V_{back} was recorded with an accuracy of $\lesssim 1 \text{ mV}$, which is required for a precise determination of the doping profile close to the Si-SiO₂ interface. In order to determine the doping density at sub-micron distances from the Si-SiO₂ interface, the measurements have to cover also positive values of V_{back} , for which the n^+p implants of Source and Drain approach forward biasing and a significant forward current is observed.

To determine the MOSFET threshold voltage, $V_{th}(V_{back})$, and the mobility of the electrons in the inversion layer, $\mu_e(V_{gate}, V_{back})$, the $I_{ds}(V_{gate}, V_{back})$ data are fitted using the standard MOSFET formula derived from the Brews charge-sheet model and a parametrisation of the dependence of the mobility on V_{gate} . The $I_{ds}(V_{gate}, V_{back})$ data are also used to determine $V_{gate}(V_{back}, N_{inv})$, the dependence of the gate voltage on the back-side voltage for constant area density of the electrons in the inversion layer, N_{inv} . The value of N_{inv} is derived from I_{ds} , taking into account the dependence of the electron mobility on V_{gate} and V_{back} .

Two methods are used to determine the doping densities for the MOSFETs with and without p -spray implant:

1. Assuming that the MOSFETs have regions of constant doping, a linear dependence of V_{th} and of $V_{gate}(N_{inv} = \text{const.})$ on $\sqrt{\Phi_S - V_{back}}$ is expected (Eq. 9), where Φ_S is the potential at the Si-SiO₂ interface. The dopant density is proportional to the square of the slope. The comparison of the slopes for V_{th} and V_{gate} for different N_{inv} values allows to check the consistency of the doping determination.
2. From the derivatives dV_{back}/dV_{th} and dV_{back}/dV_{gate} at constant N_{inv} , the depletion depth $w(V_{back})$ is derived (Eq. 13). Assuming the depletion approximation, the distance x from the Si-SiO₂ interface where the doping is determined, is equal to w . The integral of the density of holes $p(x)$ (the majority charge carriers in p -type Si), up to the distance x , $\int_0^x p(\xi) d\xi$, is proportional to the voltage differences $V_{th}(x) - V_{th}(0)$ and $V_{gate}(x) - V_{gate}(0)$ (Eq. 14). The threshold voltage corresponding to the depletion depth w is $V_{th}(w)$, the threshold voltage extrapolated to zero depletion depth is $V_{th}(0)$, and similar for $V_{gate}(x)$ for constant N_{inv} . The derivative of the integral $\int_0^x p(\xi) d\xi$ gives $p(x)$. Fitting $p(x)$ with a phenomenological function allows us to estimate the Debye correction, the difference between $p(x)$ and the doping density, and thus determine the doping profile from a sub-micron distance from the Si-SiO₂ interface to the maximum depletion depth given by the maximum $|V_{back}|$ value of the measurement. The comparison of the results obtained using V_{th} and V_{gate} for different N_{inv} values provides a check of the consistency of the doping density determination.

Method 1 is straight-forward and does not require to differentiate data points, however the value of the potential at the interface has to be assumed and the impact of the assumption of locally constant doping

is not so clear. For the MOSFET without p -spray implant it gives precise values for the doping and the oxide-charge density. For the MOSFET with p -spray implant it gives a precise value for the integrated implant dose, and approximate values for the bulk doping beyond the implant region, for the maximal implant doping density and its width.

Method 2 is more involved, as data and distributions derived from data have to be differentiated. However, it also gives more details on the doping profile. Its main assumption is the depletion approximation, and no value for the potential at the Si-SiO₂ interface has to be assumed. The dependence of $\int_0^x p(\xi) d\xi$, the integral of the majority-charge carrier (hole) density on the distance x from the Si-SiO₂ interface, is precisely determined. The hole density, $p(x)$, which is obtained by differentiation, is very sensitive to the exact knowledge of V_{back} : Changes of a single V_{back} value by 2 mV can result in changes of close-by p values by $\pm 30\%$. For M200Y, where positive V_{back} values close to forward biasing have been applied, the doping profiles at a fraction of a μm from the Si-SiO₂ interface can be determined. The typical uncertainty of $p(x)$ is $\approx 20\%$. Finally, a fit of a phenomenological parametrisation to $p(x)$ allows to apply the Debye correction to $p(x)$ and thus obtain a doping profile for the use in TCAD simulations and model calculations.

The results from both methods are consistent. To verify the methods, two MOSFETs with similar parameters as the investigated ones were simulated using Synopsys TCAD, and data with the same drain, gate and source voltages as the experimental ones have been generated. The same analysis software as for the experimental data has been used, and the results compared to the input parameters and the experimental values. For the field dependence of the electron mobility in the inversion layer, significant differences between experimental and simulated results have been found, which however should not influence significantly the extraction of the doping profiles. For distances exceeding $0.5 \mu\text{m}$ from the Si-SiO₂ interface, the extracted doping profiles for both MOSFETs are consistent with the input values. For distances smaller than $0.5 \mu\text{m}$, the doping profile extracted from the simulated data shows large unphysical fluctuations, which reflect large fluctuations of the simulated charge density distribution close to the Si-SiO₂ interface.

The work presented in this paper demonstrates how circular MOSFETs, fabricated as test structures together with sensors on high-ohmic p -type Si, can be used to determine the bulk doping as well as the doping profile of the p implants, which are required for isolating the n^+ electrodes of segmented n^+p sensors.

Acknowledgements

We thank Peter Buhmann and Michael Matysek for maintaining the measurement infrastructure of the Hamburg Detector Laboratory, where the measurements were performed in excellent shape, which is a necessary condition for the precision results presented in this paper. We thank Dr Frank Schluenzen from the DESY IT Group for setting up and maintaining the IT infrastructure used for the TCAD simulations. Ioannis Kopsalis acknowledges the fellowship by the DAAD (German Academic Exchange Service), which allowed him to obtain a PhD from the Department of Physics of the University of Hamburg.

5. List of References

References

- [1] J. Kemmer and G. Lutz, *Concepts of simplification of strip detector design and production*, Nuclear Instruments and Methods in Physics Research A 326 (1993) 209 – 213.
- [2] R. H. Richter, et al., *Strip detector design for ATLAS and HERA-B using two-dimensional device simulation*, Nuclear Instruments and Methods in Physics Research A 377 (1996) 412 – 421.
- [3] L. Andricek, et al., *Single-sided p^+n and double-sided silicon strip detectors exposed to fluences up to $2 \times 10^{14} \text{ cm}^{-2}$ 24 GeV protons*, Nuclear Instruments and Methods in Physics Research A 409 (1998) 184 – 193.
- [4] Y. Iwata, et al., *Optimal p -stop pattern for the n -side strip isolation of silicon microstrip detectors* IEEE Transactions on Nuclear Science Vol. NS-45(3) (1998) 303 – 309.
- [5] D. K. Schroder, *Semiconductor Material and Device Characterization*, Wiley-Interscience 2006.

- [6] Hamamatsu HPK, <http://www.hamamatsu.com>.
- [7] K.-H. Hoffmann, for the CMS Tracker Sensor Working Group, *Campaign to identify the future CMS tracker baseline*, Nuclear Instruments and Methods in Physics Research A 658 (2011) 30 – 35.
- [8] A. Dierlamm, for the CMS Tracker Sensor Working Group, *Characterisation of silicon sensor materials and designs for the CMS Tracker Upgrade*, Proceedings, 21st International Workshop on Vertex Detectors (Vertex 2012): Jeju, Korea, September 16 – 21, 2012, PoS Vertex 2012, p. 16.
- [9] J. Erfle, *Irradiation study of different silicon materials for the CMS tracker upgrade*, PhD thesis, University of Hamburg, 2013, DESY-THESIS 2014-010.
- [10] M. Weberpals, *Determination of the p-spray doping profile of n⁺p silicon sensors using a MOSFET*, BSC-thesis, University of Hamburg, March 2017.
- [11] J. R. Brews, *A charge-sheet model of the MOSFET*, Solid State Electronics, Vol. 21, 1978, 345 – 355.
- [12] A. S. Grove, *Physics and Technology of Semiconductor Devices*, John Wiley & Sons, Inc., 1967.
- [13] S. M. Sze, *Physics of Semiconductor Devices*, John Wiley & Sons, Inc., 1981.
- [14] I. Kopsalis, *Surface Effects in Segmented Silicon Sensors*, PhD-thesis, University of Hamburg, Jan. 2017.
- [15] C. Lombardi et al., *A Physically Based Mobility Model for Numerical Simulation of Nonplanar Devices* IEEE TRANSACTIONS ON COMPUTER-AIDED DESIGN., Vol. 7, No.11, Nov. 1988, and references therein.
- [16] E. Conwell and V. F. Weisskopf, *Theory of Impurity Scattering in Semiconductors*, Phys. Rev. 77 (1950) 388 – 390.
- [17] D. W. Feldbauer and D. K. Schroder, *MOSFET Doping profiling*, IEEE Transactions Electron. Dev. ED-38, Jan. 1991, 135 – 140.
- [18] J. M. Shannon, *D.C. Measurement of the Space Charge Capacitance and Impurity Profile Beneath the Gate of an MOST*, Solid State Electronics, Vol. 14, 1971, 1099 – 1106.
- [19] M. G. Buehler, *Dopant profiles determined from enhancement-mode MOSFET dc measurements*, Appl. Phys. Lett, Vol. 31 (12), 1971, 848 – 850.
- [20] D. P. Kennedy, P. C. Murley and W. Kleinfelder, IBM J. Res. Dev. 1968, 309.
- [21] W. E. Carter, H. K. Gummel and B. R. Chawla, *Interpretation of capacitance vs. voltage measurements of p-n junctions*, Solid State Electronics, Vol. 15, 1971, 195 – 201.
- [22] C. L. Wilson, *Correction of differential capacitance profiles for Debye-length effects*, IEEE Transactions on Electron Devices ED-27 (1980) 2262 – 2266.
- [23] Synopsys TCAD webpage: <http://www.synopsys.com>.
- [24] G. Masetti, M. Severi and S. Solmi, *Modeling of Carrier Mobility Against Carrier Concentration in Arsenic-, Phosphorus-, and Boron-Doped Silicon*, IEEE Transactions on Electron Devices ED-30, no. 7 (1983) 764 – 769.